Annular Josephson tunnel junctions in an external magnetic field: The dynamics

Nadia Martucciello and Carmine Soriano
INFM, Dipartimento di Fisica, Università di Salerno, I-84081, Baronissi, Salerno, Italy

Roberto Monaco
Istituto di Cibernetica del CNR, I-80072, Arco Felice Napoli, Italy
and INFM, Dipartimento di Fisica, Università di Salerno, I-84081, Baronissi, Salerno, Italy
(Received 15 October 1996)

We have investigated the dynamical states in annular Josephson tunnel junctions in the presence of an externally applied uniform magnetic field parallel to the barrier plane. For electrically small and overdamped junctions we show that the Kulik perturbative theory for the Fiske singularities can easily and successfully be extended to the annular geometry even in the case of trapped fluxons. For electrically long annular junctions we present the results of the numerical simulations. Further, we report on the magnetic-field dependence of the amplitude of the so-called Fiske steps in specially designed high dissipation Nb/Al-AlO_x-Al/Nb annular junctions having different normalized circumferences. [S0163-1829(97)04517-7]

I. INTRODUCTION

Annular, i.e., ring-shaped Josephson tunnel junctions show a large variety of interesting physical phenomena due to the fluxoid quantization in a superconducting ring and due to the absence of boundaries;[1] they are a topic of current experimental interest. Recently, the static properties of annular Josephson tunnel junctions in the presence of uniform magnetic field applied in the plane of the tunnel barrier have been extensively examined by Martucciello and Monaco[2,3] and by Vernik *et al.*[4] In Ref. 2, the dependence of the critical current on a uniform magnetic field for annular Josephson tunnel junctions having different geometrical configurations was investigated both experimentally and numerically. Among other things, it was found that when the normalized ring circumference is less than unity, i.e., the physical length is less than the Josephson penetration depth λ_j, the I_c vs H follows an nth order Bessel function behavior, where n is the number of fluxons trapped in the barrier. For longer junctions numerical[2,4] and analytical[3] solutions of the appropriate perturbed sine-Gordon equation (PSGE) show that a barrier-parallel magnetic field produces potential wells at diametrically opposite points where static fluxons and antifluxons align with the external field.

In this paper we shall extend our study to the dynamic properties of both electrically small ($2\pi\overline{r}<\lambda_j$) and long ($2\pi\overline{r}>\lambda_j$) annular Josephson tunnel junctions in the presence of an external magnetic field applied in the plane of the barrier. So far the fluxon dynamics in annular junctions has been studied in a number of papers[1,5–12] but only in the case of no externally applied field, i.e., only the so-called zero-field singularities (ZFS's) were considered in the ring I-V characteristic (IVC). We provide, instead, a study of the Fiske singularities (FS) in annular junctions, i.e., of those steps that, as in the case of more conventional, linear junctions with open boundary conditions, appear on the junction IVC as a result of the application of an external field in the plane of the barrier[13].

The paper is organized as follows. In Sec. II we present a theoretical approach to the problem that can be solved by extending the Kulik theory[14] to annular junctions, in other words, by means of a perturbative analysis it is possible to linearize the system and to find the theoretical dependence of the FS amplitude on the magnetic field for small and underdamped junctions; further, for long junctions we show the results of numerical simulations. In Sec. III we describe the particular fabrication process that has been adopted to realize high-loss Nb/Al-AlO_x-Al/Nb annular Josephson tunnel junctions and we present the experimental results for the magnetic dependence of the FS amplitude. Some conclusions are drawn in Sec. IV. In the Appendices we present, in some detail, the calculations for the perturbative theory.

II. THEORETICAL ANALYSIS

A. Derivation of the model

The description of an annular junction in the presence of a uniform externally applied magnetic field is done using cylindrical coordinates r, θ, and z, assuming that the junction lies in the $z=0$ plane and its center of symmetry is located at $r=0$, as shown in Fig. 1; the origin of the angular abscissa, i.e., $\theta=0$ is set in the direction of the field. Further, let us call r_o and r_i the outer- and inner-ring radius, respectively, and let us assume that the ring width $\Delta r=r_o-r_i$ is much smaller than both the mean radius $\overline{r}=0.5(r_o+r_i)$ and the Josephson penetration length λ_j, so that we are dealing with a one-dimensional junction. Using a Lagrangian formalism Grønbech-Jensen *et al.*[15] have shown that the phase difference ϕ of the macroscopic superconducting quantum mechanical wave function measured across the barrier of an annular Josephson tunnel junction in a uniform magnetic field parallel to the barrier plane obeys the following perturbed sine-Gordon equation (PSGE):

$$\phi_{xx}-\phi_{tt}-\sin\phi=-\gamma-\eta\Delta\sin kx+\alpha\phi_t-\beta\phi_{xxt}, \quad (1)$$

in which the dimensionless angular coordinate $x=\overline{r\theta}/\lambda_j$ has been introduced and the time has been normalized to the

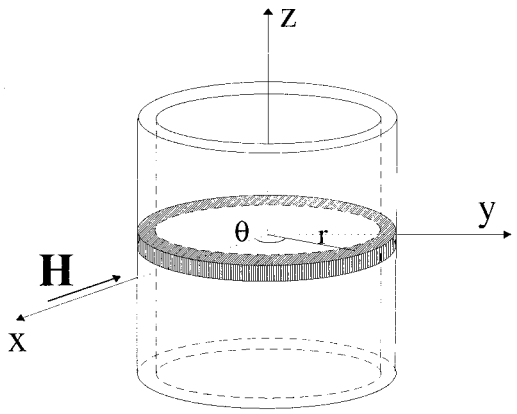

FIG. 1. Schematic drawing of an annular junction. The origin of the angular abscissa, i.e., $\theta=0$, is set in the direction of the external field **H**.

inverse of the junction plasma frequency. γ is the distributed bias current normalized to $I_{c0}=2\pi J_c\overline{r\Delta r}$ (where J_c is the uniform maximum Josephson current density), η is the field amplitude normalized to $\Phi_0/2\pi\mu_0\overline{rd}$, Δ is the coupling between the external field and the flux density in the junction, and $k=2\pi/l$ is a dimensionless wave number, $l=C/\lambda_j$ being the normalized ring circumference. α and β are the loss coefficients due to the tunneling current and to the surface impedance, respectively. In Ref. 2, Eq. (1) was obtained imposing the continuity of the induction field **H** on the junction boundary, through[16,17]

$$\nabla(\phi+\beta\varphi_t)=\frac{2\pi d\mu_0}{\Phi_0}\mathbf{H}\times\mathbf{u}_z$$

($\mathbf{u}_z$ is a unit vector in the z direction) and it was found that Δ is a geometrical factor that depends on the particular junction configuration and is inversely proportional to l^2. The boundary conditions for Eq. (1) are periodic[1] and derive from fluxoid quantization:[2]

$$\phi(x+l)=\phi(x)+2\pi n, \tag{2}$$

where n is an integer corresponding to the number of fluxons trapped in the junction barrier at the normal-superconducting transition; n is a topological system constant, that is, only fluxon-antifluxon pairs can be created or annihilated as long as the junction remains in the superconducting state. In[2] the static PSGE, that is,

$$\phi_{xx}-\sin\phi=\gamma-\eta\Delta\sin kx, \tag{3}$$

was solved numerically (with $\Delta=k^2$) for different values of the normalized circumference l and, in particular, the magnetic patterns $\gamma_c(\eta)$ were found for $l=6$, 12, and 24. When static solutions were computed numerically, we found that, for a given field, different phase profiles are possible depending on the number of fluxon-antifluxon pairs nucleated at two diametrically opposed points in the barrier where the effect of the field is largest. In Ref. 3 a perturbative analysis of Eq. (3), with n set equal to 0, has been carried out based on the ansatz $\phi=\phi^0+\phi^1$, where ϕ^0 is known and ϕ^1 is small in comparison to ϕ^0; the analytical results fit the numerical results well in cases of small normalized ring lengths or large external fields. Experimental data on high-quality Nb/Al-AlO_x-Al/Nb junctions support the theoretical analysis provided current limiting static self-field effects are taken into account in real devices,[2] also in the case when $n\neq 0$.[4]

B. Perturbative analysis

The study of the statics[2,3] suggests as a zero order approximation ϕ^0 for the solution of Eq. (1) which satisfies the boundary condition Eq. (2):

$$\phi^0=nkx+\eta\sin kx+\omega t, \tag{4}$$

where the first term represents the linear phase twist due to the presence of n fluxons trapped in the barrier, the second term takes into account the potential created by the external magnetic field, and ωt is a uniform rotating term, with $\omega=\langle\phi_t\rangle$ being the normalized junction voltage ($\langle\rangle$ means the average with respect to both space and time). Since we are interested in the stationary solutions of Eq. (1), we have neglected in Eq. (4) the presence of a constant term in the expression for ϕ^0. We expand the exact solution of Eq. (1) around the rotating solution Eq. (4) as $\phi=\phi^0+\phi^1$, with the assumption that $|\phi^1|\ll 1$ so that $\sin\phi\simeq\sin\phi^0+\phi^1\cos\phi^0$ and obtain the following linear PDE (partial derivative equation) for ϕ^1:

$$\phi^1_{xx}-\phi^1_{tt}-\sin\phi^0-\phi^1\cos\phi^0=-\gamma+\alpha\omega+\alpha\phi^1_t-\beta\phi^1_{xxt} \tag{5}$$

with the following periodic boundary conditions:

$$\phi^1(x+l)=\phi^1(x). \tag{6}$$

Further, $\langle\phi^1_t\rangle=0$. The spatial Fourier expansion of the periodic function ϕ^1 is

$$\phi^1=\sum_{m=1}^{\infty}[F_m(t)\cos mkx+S_m(t)\sin mkx] \tag{7}$$

with $F_m(t)=A_m\cos\omega t+B_m\sin\omega t$ and $S_m(t)=C_m\cos\omega t+D_m\sin\omega t$. Expanding $\sin\phi^0$ in a Fourier-Bessel series and using the orthogonality of trigonometric functions, it is possible to find the expression for the coefficients A_m, B_m, C_m, and D_m (see Appendix A). It is easy to show that both $|F_m|$ and $|S_m|$ are inversely proportional to Δ_m and that the mth term in the sum Eq. (7) is

$$\phi^1_m=\Delta_m^{-1}[J_{m+n}(\eta)\cos(\omega t-mkx+\delta_m)+J_{m-n}(\eta)\cos(\omega t+mkx+\delta_m)], \tag{8}$$

where $J_n(\eta)$ are the Bessel functions of integer order n and argument η. Further, $\Delta_m^2=(m^2k^2-\omega^2)^2+\omega^4/Q_m^2$ and $\tan\delta_m=Q_m[1-(mk/\omega)^2]$; we have introduced the very important dimensionless quality factors $Q_m^{-1}=Q_\alpha^{-1}+Q_\beta^{-1}=(\alpha+\beta m^2k^2)/\omega$, which give a measure of the junction losses and depends on the junction voltage. Equation (8) can be interpreted physically as the superposition of two small amplitude waves traveling with equal but opposite speeds. The requirement that ϕ^1 be small implies that the present approach is valid whenever, for all integers m, $\Delta_m\gg 1$, i.e., when

$$Q_m\ll\omega^2. \tag{9}$$

Recalling the Bessel function asymptotic expansion for large arguments $J_m(\eta) \simeq \sqrt{2/(\pi\eta)}\cos(\eta - m\pi/2 - \pi/4)$, we note that the ϕ_m^1 are always small in the large field limit $\eta \gg 1$. The *I-V* curve comes from the dc part of Eq. (5) as

$$\gamma = \alpha\omega + \langle \phi^1 \cos\phi^0 \rangle. \tag{10}$$

The first term in Eq. (10) represents the ohmic part of the *I-V* characteristic, while the second term corresponds to the dc normalized Josephson current $i = \langle \sin\phi \rangle$. Inserting the expression for ϕ^0 and ϕ^1 and carrying out the calculations, we end up with (see Appendix B)

$$i(\omega,\eta) = \sum_{m=1}^{\infty} \frac{[J_{m+n}^2(\eta) + J_{m-n}^2(\eta)]}{2\omega^2} \times \frac{Q_m^{-1}}{[(mk/\omega)^2 - 1]^2 + Q_m^{-2}}. \tag{11}$$

The Josephson current is given by an infinite series of equidistant resonances at $\omega = mk = 2\pi m/l$, whose maximum amplitudes are:

$$I_{m,n}^{\max}(\eta) = I_{c0} \frac{Q_m}{m^2k^2} \frac{J_{m+n}^2(\eta) + J_{m-n}^2(\eta)}{2}. \tag{12}$$

With $\omega = mk$ the inequality Eq. (9) implies that the limit of validity of this perturbative approach is set by

$$Q_1 \ll \frac{2\pi\lambda_j}{C}, \tag{13}$$

that is, either when the junction is electrically short or when the losses are large. However, for long and/or underdamped junctions the theory should apply only for those Fiske steps whose order m is so large that $mk(\alpha + \beta m^2 k^2) \gg 1$. Further, for the mth FS, the main contribution to ϕ^1 in the sum Eq. (7) is given by Eq. (8) with $\omega = mk$:

$$\phi_m^1(x,t) = \frac{Q_m}{m^2k^2}[\pm J_{m+n}(\eta)\cos mk(t-x) \pm J_{m-n}(\eta)\cos mk(t-x)]. \tag{14}$$

This is a standing wave obtained from the superposition of two traveling waves having opposite speeds; the standing wave ratio $(|J_{m+n}(\eta)| + |J_{m-n}(\eta)|)/(|J_{m+n}(\eta)| - |J_{m-n}(\eta)|)$ strongly depends on the field amplitude. It is clear that, in the range of validity of the perturbative analysis, a wavelike description of the fluxon dynamics is more appropriate than a particlelike description, since in a small junction a fluxon can be seen as a distributed, rather than localized, phase twist of 2π.

In the case of no trapped fluxons ($n = 0$), we end up with the following field dependence for the maximum normalized amplitude of the mth FS, that is very similar to that found for rectangular junctions[18]:

$$i_{m,0}(\eta) = \frac{I_{m,0}^{\max}(\eta)}{I_{c0}} = \frac{Q_m}{m^2k^2} J_m^2(\eta). \tag{15}$$

From the expression of the quality factors Q_m, we note that if the surface loss dominates the tunneling loss (for example, at high voltages or at low temperatures), then in the last expression the coefficient in front of the squared Bessel function decreases as the third power of the step order m; in other words, the FS amplitude decreases very fast as we move to large step orders. In the large field limit, Eq. (15) can be written in terms of damped trigonometric functions:

$$i_{m,0}(\eta) \simeq \frac{Q_m}{m^2k^2} \frac{2}{\pi\eta} \cos^2\left(\eta - \frac{m\pi}{2} - \frac{\pi}{4}\right). \tag{16}$$

As a further example of the usefulness of Eq. (12), we consider the case of a single trapped fluxon ($n = 1$) traveling around the ring; the magnetic-field dependence of the maximum amplitude of the step associated with this dynamical state is given by

$$I_{1,1}^{\max}(\eta) = I_{c0} \frac{Q_1}{k^2} \frac{J_0^2(\eta) + J_2^2(\eta)}{2}. \tag{17}$$

For $\eta = 0$, Eq. (17) gives the zero-field amplitude of the single fluxon step and Eq. (14) states that the corresponding dynamical state is simply a wave travelling around the ring. Equation (12) and Eq. (14) give similar results when applied to the general case $m = n$.

C. Numerical simulations

In an effort to obtain further insight into the dynamics of this system we have carried out detailed numerical simulations of Eq. (1), using a fourth-order Runge-Kutta algorithm on a spatially discretized counterpart, for different values of the normalized ring circumference l. The loss parameters α and β were set equal to 0.1 and 0.01 respectively. We calculated a number of IVC's of annular junctions with no trapped fluxons, that is, with $n = 0$ in the boundary condition Eq. (2). We found that field induced current singularities, that is, Fiske steps indeed occurred at normalized voltages $\omega_m = 2\pi m/l$ indicating that, on the average, m fluxons and/or antifluxons travel around the ring when the junction is biased on the mth order step; it should be recalled in this regard, that, although the Lorentz force due to the bias current acts in opposite directions for fluxons and antifluxons, the voltage drops due to traveling fluxons and antifluxons have the same sign and add up. In Figs. 2(a)–(d) we show the numerically computed magnetic-field dependence of the amplitude of the first three FS for l equal to 1, 3, 6, and 12. In all figures the data relative to the first, second, and third FS are shown by open circles, closed circles, and stars, respectively. These data are compared with the perturbative analysis expression Eq. (15), although, for the given α, β, and l, the Q_1/k^2 ratios are equal to 0.36, 3.4, 9.1, and 20 for l equal to 1, 3, 6, and 12, respectively, so that a good fit between the theory and the simulation can be expected only in Fig. 2(a) for $l = 1$. Further, both the horizontal and vertical scale ranges change from figure to figure in order to better present the data. In Fig. 2(a) the data (both numerical and theoretical) relative to the height of second and third FS have been scaled by a factor 10 and 30, respectively. As expected, for $l = 1$, we get an excellent fit between the numerical data and the theoretical expression for $n = 1$, 2, and 3, since the Q_1/k^2 ratio is smaller than unity; further, we observe an increasing departure of the theory from simulation as we

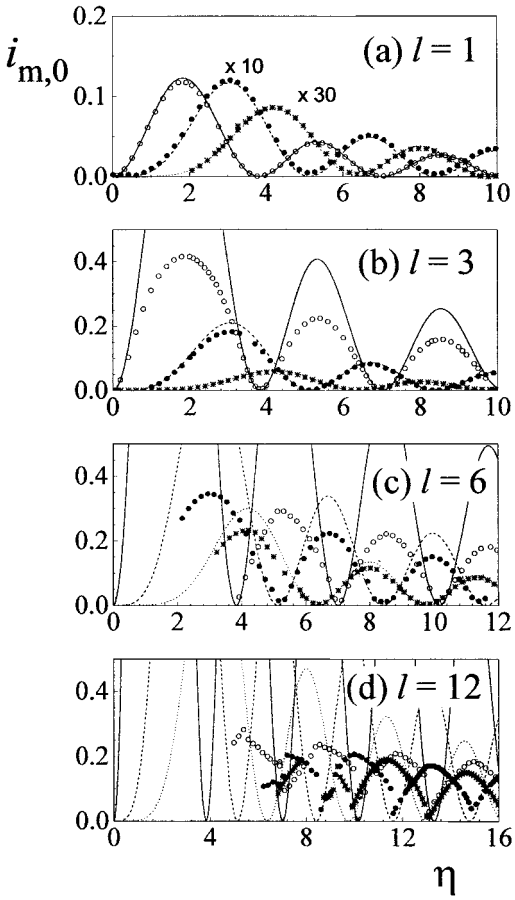

FIG. 2. Magnetic pattern of the FS amplitudes for annular junctions in a barrier-parallel magnetic field for different normalized ring circumferences l. The data are obtained from the numerical integration of Eq. (1) with $\alpha=0.1$, $\beta=0.01$ and $n=0$; the data relative to FS1, FS2, and FS3 are shown with open circles, closed circles, and stars, respectively. The lines are the theoretical curves for different values of the step order m according to Eq. (15).

move to large Q_1/k^2 ratios, although the fit is still reasonably good for second and third steps in the case of $l=3$ and for the third step in the case of $l=6$. There are at least two other features that should be noted in the numerical data shown in Fig. 2. (i) as we move to large l, the field values which yield the minima (the zeroes) and the maxima in the FS magnetic patterns do not change, however, the step amplitudes increase and the increment is more pronounced for the higher order steps. (ii) for $l=6$ data are missing in the small field region, the situation is even worse for $l=12$. The lack of FS for small field has been observed experimentally on long linear junctions[19,20] and, as we will see in the next section, is typical of long annular junctions too. In order to test the perturbative theory also in the case of trapped fluxons, we have integrated Eq. (1) with $n=1$, $l=3$, $\alpha=0.1$, and $\beta=0.01$ and we have monitored the amplitude of the FS associated with the single fluxon motion as a function of the applied field. This dependence is reported in Fig. 3, where the points correspond to the numerical data and the full line to Eq. (17) with $Q_1/k^2=3.4$; although we are out of the validity range of the perturbative theory $Q_1/k^2>1$, there is at least a good qualitative agreement.

In order to shed some light on the mechanism responsible for the appearance of the FS's, we have observed the time

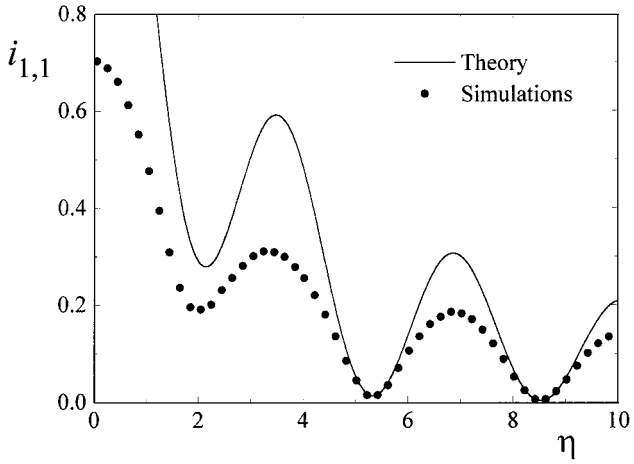

FIG. 3. Magnetic pattern of the single-fluxon FS amplitude for annular junctions in a barrier-parallel magnetic field. The data are obtained from the numerical integration of Eq. (1) with $\alpha=0.1$, $\beta=0.01$, $l=3$, and $n=1$. The full line is the theoretical curve according to Eq. (17).

evolution of the phase with the junction biased on the first and second FS. In a stationary state the phase time evolution is periodic with a period $T=l/m$. Since both the three-dimensional plot of $\phi(x,t)$ and the snapshots of $\phi(x)$ at different time intervals are not easy to understand, we have decided to make use of the simple, qualitative drawings

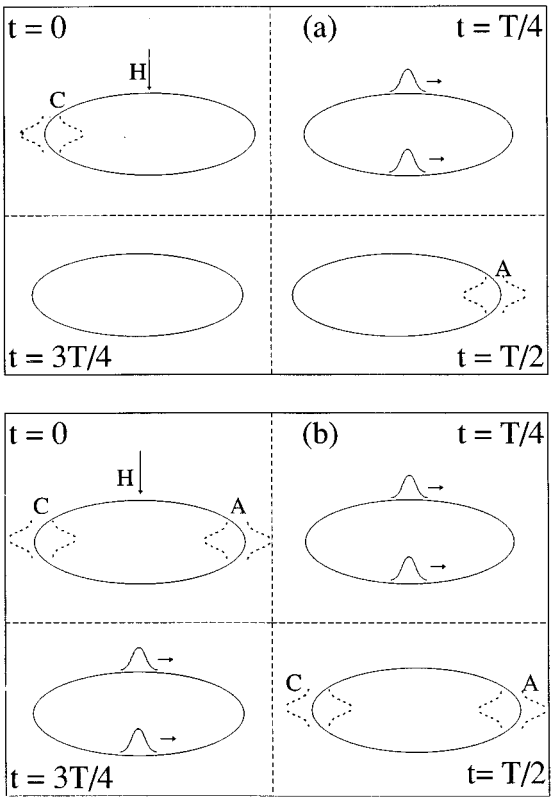

FIG. 4. Sketch of the dynamical states observed on annular junctions biased on the first (a) and second (b) Fiske step. Fluxons (antifluxons) are drawn outside (inside) the ring. The point where the fluxon-antifluxon pairs are created (annihilated) is indicated with C (A).

shown in Fig. 4(a) and Fig. 4(b) for the dynamical states observed in the case of the first and second Fiske step, respectively. In the case of the first Fiske step the dynamics can be described as follows. At $t=0$, a fluxon-antifluxon pair is created at $\theta=-\pi/2$; under the influence of the Lorentz forces due to the bias current and the external magnetic field, the fluxon and the antifluxon start to move in opposite directions and annihilate at $\theta=+\pi/2$ after about a half period; during the second half of the period no traveling fluxon (or antifluxon) are observed until a new fluxon-antifluxon pair is created at $t=T$ and so on. According to this picture, the average number of traveling fluxons is one, so that the voltage expected for this dynamical step is the same as that for the single fluxon step. As far as the second Fiske step is concerned, the dynamics is a little bit more complicated [see Fig. 4(b)]: at $t=0$ while a fluxon-antifluxon pair is created in at $\theta=-\pi/2$ a second pair is annihilated at $\theta=\pi/2$; the fluxon and the antifluxon move toward the annihilation point and reach it at $t=T/2$ while a new pair is created at $\theta=-\pi/2$; the dynamics in the second half of the period is exactly equal to that in the first half period. According to this picture, the average number of traveling fluxons is two, so that, the voltage expected for this dynamical step is twice that of the first Fiske step. We would like to observe that other mechanisms exist that would give the voltage of the second Fiske singularity, but we only observed the one described above. When the field is larger than the critical value, as we know from the study of the static properties,[2] static fluxons and antifluxons sit in the potential wells at $\theta=0$ and $\theta=\pi$, respectively; the number of fluxons goes as the lobe order in the magnetic pattern. We want to stress that, although in Figs. 4(a) and 4(b) we have depicted the fluxons as particles, a description in terms of waves is more realistic also in the case of very long junctions for which the Fiske steps are observed for field values so large to penetrate in the barrier and to produce a phase twist.

III. EXPERIMENTS

A. The samples

Two processes have been used to fabricate Nb/Al-AlO_x-Al/Nb junctions. The first one is the well known selective niobium anodization process (SNAP)[21] that, as all the other processes based on the Nb/Al-AlO_x-Al/Nb trilayer deposition, provides high-quality junctions, i.e., having extremely low losses $Q_1 \gg 1$;[22] further, with this technology it is difficult to get Josephson current densities lower than 100 A/cm^2,[23] i.e., Josephson penetration depths larger than 100 μm. In other words, in order to satisfy the condition Eq. (13), annular junctions with very small physical circumference are required, but then the condition of unidimensionality $\Delta r \ll \overline{r}$ cannot be satisfied with a standard 1-μm-resolution photolitographic process. Furthermore, because of the low barrier loss, the I-V characteristic of high-quality junctions shows a wide region of instability near $V=0$ that often prevents biasing the junction onto the low-order current singularities, in particular for low values of the applied field. This region of instability that was theoretically investigated by Costabile *et al.*[24] for long linear overlap-type junctions (with no magnetic field) and was experimentally found to be more pronounced in long junctions having annular geometry. To overcome the problems related to the low barrier losses and to the small Josephson penetration depths, we developed a new fabrication process not based on the trilayer deposition that will be referred to as the low-Q process (LQP) and is illustrated in Fig. 5. Initially, a Nb film is deposited on the whole wafer and patterned with the geometry of the junction base electrode by means of CF_4 reactive ion etching [Fig. 5(a)]. Afterward, the junction area is defined by a resist stencil [Fig. 5(b)] which protects the base electrode against the niobium liquid anodization [Fig. 5(c)]. Finally, after a soft argon sputter cleaning of the base electrode surface, a Al-AlO_x-Al/Nb bilayer is deposited and patterned with the geometry of the counter electrode by means of CF_4 reactive ion etching or lift-off technique [Fig. 5(d)]. The details of the film deposition and etching and of the niobium anodization can be found elsewhere.[25] A typical I-V curve of a small Josephson tunnel junction fabricated with the SNAP process and the LQP process are shown in Fig. 6(a) and Fig. 6(b), respectively. We observe that the LQP process yields junctions with larger subgap currents (quality factor $V_m \simeq 10$ mV) when compared to typical junctions fabricated with SNAP technology; furthermore, the I_cR_n product and the gap voltage are lower, i.e., 0.4 and 2.4 mV, respectively. The junction quality has been found to be strictly related to the Nb sputter etching parameters, although a systematic work to establish the exact correspondence has still to be done.

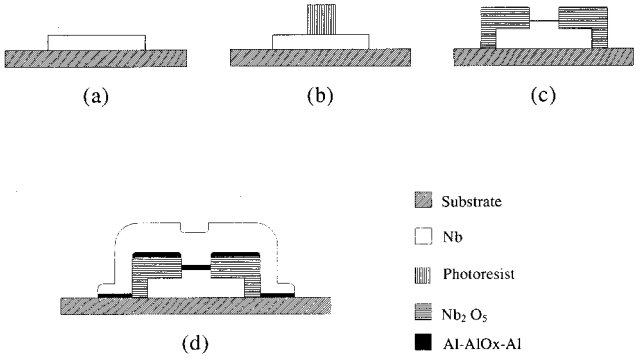

FIG. 5. Low-Q Process (LQP) used to fabricate high loss Nb/Al-AlO_x-Al/Nb junctions. (a) Nb base electrode deposition and patterning; (b) and (c) definition of the junction area by Nb liquid anodization; (d) deposition of the Al-AlO_x-Al/Nb bilayer.

We believe that we are dealing with superconductor–normal-metal–insulator–superconductor junctions where the normal layer is mainly provided by the disordered Nb surface after the sputter cleaning of the base electrode. This implies that the junction magnetic penetration is larger and, as we will see in the next paragraph, the Swihart velocity is lower. Further, the magnetic pattern of the maximum critical current of small square test junctions was Fraunhofer-like with equally spaced and well-pronounced minima indicating that Nb-insulator barrier is uniform and pinhole-free. The LQP process is easy and very reliable; a deeper understanding of the properties of the junctions fabricated with the LQP will be the subject of a future work.

B. Experimental results

In this section, we present the results obtained for short annular junctions fabricated with the low-Q process and hav-

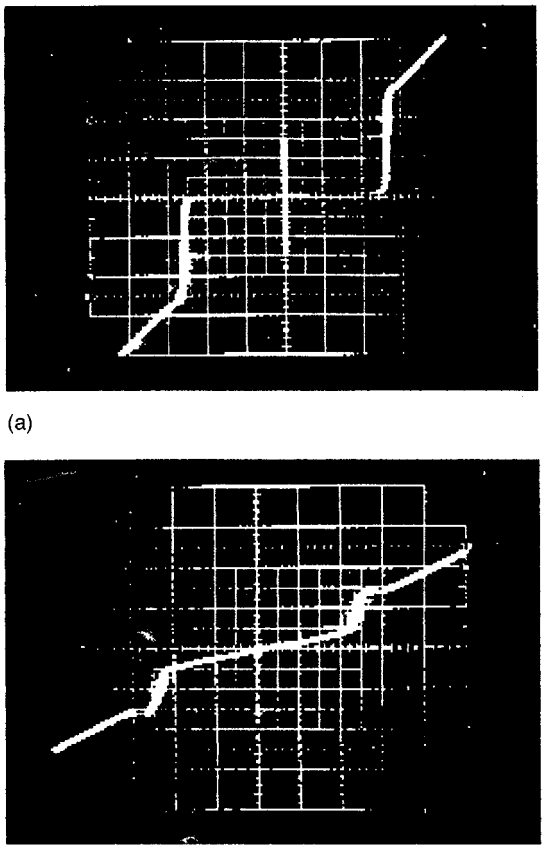

FIG. 6. Typical I-V characteristics of junctions fabricated with (a) selective niobium anodization process and (b) low-Q process. Horizontal scales: 1 mV/div.

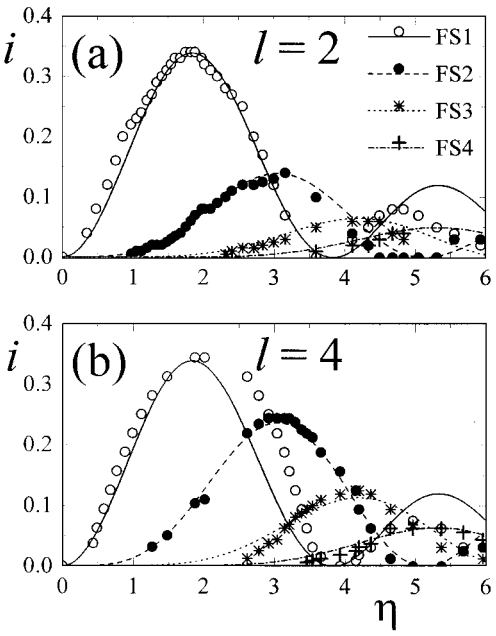

FIG. 7. Experimental patterns of the FS amplitudes for annular junctions fabricated with the LQP in a barrier-parallel magnetic field for different normalized ring circumferences l. The lines are the theoretical curves for different values of the step order m according to Eq. (15).

ing a mean circumference $C=500$ μm and ring width $\Delta r=30$ μm. Critical current densities as low as 5 A/cm^2 were obtained corresponding to Josephson penetration depths as large as 250 μm. Upon application of a magnetic field in the plane of the barrier, almost equally spaced Fiske resonances appeared on the I-V curve, as expected, at quantized asymptotic voltages $V_n=n\Phi_0\overline{c}/C$. We found that these voltages are independent of the field orientation provided in the plane of the barrier. In Fig. 7 we present the magnetic field dependence of the maximum amplitude of the first four Fiske singularities for two junctions having different normalized ring circumferences, viz., $l\simeq 2$ and $l\simeq 4$ in Fig. 7(a) and Fig. 7(b), respectively. The experimental points for different step orders are represented with different symbols, as shown in the legend. Further, in order to evidence the J_m^2 dependence, we show with lines the theoretical fit according to Eq. (15) with arbitrarily chosen prefactors Q_m/m^2k^2. In fact, as in the case of rectangular junctions,[26] Q_m must be considered as some phenomenological parameter to be found experimentally, for example, from the width of the resonance maxima; once the Q_m are known for different m, an estimation of the loss coefficients α and β can be attempted. We plan to find these coefficients for LQP samples in a future work and to relate them to the different conditions of fabrication. As far as these data are concerned the factors which give the best fit for the first Fiske step is $Q_1/k^2\simeq 1$ for both the samples, meaning that the junctions are quite small and underdamped, but not enough to satisfy the criterion of application of the Kulik theory. For slightly longer ($l\simeq 8$) and very long ($l\simeq 30$) annular junctions (fabricated with SNAP or LQP) we found a situation very similar to the numerical one: for low field values the Fiske singularities were absent or very tiny and suddenly increased for a given field value that depends on the step order and on the junction length; the longer the junction, the larger this threshold value. We believe that this threshold field is approximatively equal to the junction critical field which was found to depend quadratically on the normalized ring circumference both from the numerical simulations[2] and from theoretical considerations.[3] For field values larger than this threshold the dependence is regular and Bessel-like. We would like to point out that these observations have been made by other authors on rectangular junctions too.[19,20] Finally, for very large field values, we have observed the alternation of even and odd steps as foreseen by Eq. (16).

IV. DISCUSSION AND CONCLUSION

We have demonstrated that the Kulik theory,[14] that describes the phase dynamics in electrically short, rectangular Josephson tunnel junctions in the presence of an external magnetic field, can be successfully extended to underdamped annular junctions; an extension of the Kulik theory to high-Q annular junctions will be attempted in the future. The main results of this perturbative approach are: (i) the dynamics of a annular junction can be described by the superposition of two small amplitude waves traveling in opposite directions; (ii) the maximum amplitude of the Fiske step follows a Bessel function dependence on the external field. We believe that Eq. (12) is particularly useful in the context of particle

detectors in which the Josephson current and the resonant steps in the low voltage range have to be depressed by means of large external field that may deteriorate the superconducting properties of the electrodes. Since the winding number (i.e., the difference between the number of fluxons and the number of antifluxons) which is proportional to the trapped magnetic flux is a topological constant, Eq. (12) states that if an annular junction has trapped n fluxons at the time of the transition to the superconducting state, then the first $n-1$ steps will be vanishingly small without the need to apply an external field; further, the zero-voltage critical current will be vanishingly small as well, as already demonstrated theoretically[3] and experimentally.[4]

The numerical integration of the perturbed sine-Gordon equation has shown that the magnetic-field dependence of the field induced current steps is Bessel-like also for electrically long junctions. Further, the dynamics can be described in terms of nucleation and destruction of fluxon-antifluxon pairs.

In order to obtain an experimental confirmation of the Kulik theory we have developed a new fabrication process that produces underdamped junctions; it is generally found that the main losses are related to the surface impedance of the superconducting films and to the quasiparticle tunneling current. Losses in the dielectric layer due to radiation from the junction can be shown to be negligible; also geometric contributions to the quality factor due to the edge defects of the junction are not relevant for samples of rather large size and with annular geometry. For high-quality devices, the contribution to the losses due to quasiparticle tunnel is negligible in the frequency range and at the temperature considered, however, we believe that this is no longer true for LQP junctions. In a future work, by carefully recording the step profiles, it will be possible to determine the contributions to total losses coming from the the surface impedance of the superconducting films and from the quasiparticle tunneling current.

APPENDIX A: CALCULATION OF ϕ^1

We start from Eq. (1) with the boundary conditions given by Eq. (2) and we assume that $\phi=\phi^0+\phi^1$, where $\phi^0=nkx+\eta\sin kx+\omega t$. Inserting the last two expressions in Eq. (1), we end up with a linear PDE Eq. (5) for ϕ^1 that we assume to be of the form given in Eq. (7). By means of algebraic calculations it is possible to find the Fourier expansions of $\sin\phi^0$ and $\cos\phi^0$:

$$\sin\phi^0=\sum_{m=1}^{\infty}(d_m\cos mkx\sin\omega t+c_m\sin mkx\cos\omega t), \tag{A1}$$

$$\cos\phi^0=\sum_{m=0}^{\infty}(d_m\cos mkx\cos\omega t-c_m\sin mkx\sin\omega t), \tag{A2}$$

with

$$c_m=J_{m-n}(\eta)-J_{m+n}(\eta) \tag{A3}$$

and

$$d_m=J_{m-n}(\eta)+J_{m+n}(\eta), \tag{A4}$$

where $J_n(\eta)$ are the Bessel functions of integer order n and argument η. We would like to observe that also $\sin\phi^0$ can be seen as a superposition of waves traveling with opposite speeds; in fact, Eq. (A1) can be written as

$$\sin\phi^0=\sum_{m=0}^{\infty}[J_{m+n}(\eta)\cos(\omega t-mkx)+J_{m-n}(\eta)\cos(\omega t+mkx)].$$

Considering that $F_m''=-\omega^2F_m$ and $S_m''=-\omega^2S_m$, substituting Eq. (7), Eq. (A1), Eq. (A3), and Eq. (A4) in Eq. (5) and using the orthogonality of trigonometric functions, we obtain

$$(m^2k^2-\omega^2)F_m+(\alpha+\beta m^2k^2)F_m'=-d_m\sin\omega t, \tag{A5}$$

$$(m^2k^2-\omega^2)S_m+(\alpha+\beta m^2k^2)S_m'=-c_m\cos\omega t. \tag{A6}$$

From Eq. (A5), we have

$$(m^2k^2-\omega^2)B_m-\omega(\alpha+\beta m^2k^2)A_m=-d_m,$$

$$\omega(\alpha+\beta m^2k^2)B_m+(m^2k^2-\omega^2)A_m=0.$$

By solving the system, we obtain the following expression for the coefficients A_m and B_m:

$$A_m=\frac{d_m\omega Q_m^{-1}}{\Delta_m^2}$$

and

$$B_m=-\frac{d_m(m^2k^2-\omega^2)}{\Delta_m^2}. \tag{A7}$$

Analogously, from Eq. (A6), we can find the coefficients C_m and D_m, which are

$$C_m=-\frac{c_m(m^2k^2-\omega^2)}{\Delta_m^2}$$

and

$$D_m=-\frac{c_m\omega Q_m^{-1}}{\Delta_m^2}, \tag{A8}$$

where $Q_m^{-1}=(\alpha+\beta m^2k^2)/\omega$ and $\Delta_m^2=(m^2k^2-\omega^2)^2+\omega^4/Q_m^2$.

APPENDIX B: CALCULATION OF $\langle\sin\phi\rangle$

In order to calculate the Josephson current, we have to calculate the time and space average of $\sin\phi$, by making use of Eq. (7) and Eq. (A2):

$$
\begin{aligned}
i &= \langle \sin\phi \rangle = \langle \phi^1 \cos\phi^0 \rangle \\
&= \lim_{T\to\infty} \int_0^T \frac{dt}{T} \int_{-l/2}^{l/2} \frac{dx}{l} \phi^1 \cos\phi^0 = \frac{1}{4} \sum_{m=1}^{\infty} (A_m d_m - D_m c_m) \\
&= \frac{1}{4} \sum_{m=1}^{\infty} \left[\frac{\omega d_m^2 (\alpha + \beta m^2 k^2)}{\Delta_m^2} + \frac{\omega c_m^2 (\alpha + \beta m^2 k^2)}{\Delta_m^2} \right] \\
&= \frac{1}{2} \sum_{m=1}^{\infty} \left[[J_{m+n}^2(\eta) + J_{m-n}^2(\eta)] \frac{\omega(\alpha + \beta m^2 k^2)}{\Delta_m^2} \right].
\end{aligned}
$$

Finally, introducing the Q factors, we can write the normalized Josephson current carried on the Fiske steps as an explicit function of the step voltage and of the external field:

$$
\begin{aligned}
i(\omega, \eta) = \sum_{m=1}^{\infty} & \frac{[J_{m+n}^2(\eta) + J_{m-n}^2(\eta)]}{2\omega^2} \\
& \times \frac{Q_m^{-1}}{[(mk/\omega)^2 - 1]^2 + Q_m^{-2}}.
\end{aligned}
$$

[1] D. W. McLaughlin and A. C. Scott, Phys. Rev. A **18**, 1652 (1978).

[2] N. Martucciello and R. Monaco, Phys Rev. B **53**, 3471 (1996).

[3] N. Martucciello and R. Monaco, Phys Rev. B **54**, 9050 (1996).

[4] I. V. Vernik, S. Keil, N. Thyssen, T. Doderer, A. V. Ustinov, H. Kohlstedt, and R. P. Huebener, Proceedings of the 21st International Conference on Low Temperature Physics, Prague; LT21, part S2, Superconducitivity 1: LTS–Tunneling Phenomena, pp. 649–650 (1996).

[5] B. Dueholm, A. Davidson, C. C. Tsuei, M. J. Brady, K. H. Brown, A. C. Callegari, M. M. Chen, J. H. Greiner, H. C. Jones, K. K. Kim, A. W. Kleinsasser, H. A. Notarys, G. Proto, R. H. Wang, and T. Yogi, *Proceedings of LT-17*, edited by U. Eckerm, A. Schmid, W. Weber, and H. Wuhl (Elsevier, New York, 1984).

[6] A. Davidson, B. Dueholm, B. Kryger, and N. F. Pedersen, Phys. Rev. Lett. **55**, 2059 (1985).

[7] A. Davidson, B. Dueholm, and N. F. Pedersen, J. Appl. Phys. **60,** 1447 (1986).

[8] A. V. Ustinov, T. Doderer, R. P. Huebener, N. F. Pedersen, B. Mayer, and V. A. Oboznov, Phys. Rev. Lett. **69**, 1815 (1992).

[9] I. V. Vernik, V. A. Oboznov, and A. V. Ustinov, Phys. Lett. A **168**, 319 (1992).

[10] A. Laub, T. Doderer, S. G. Lachenmann, R. P. Huebener, and V. A. Oboznov, Phys. Rev. Lett. **75**, 1372 (1995).

[11] I. V. Vernik, N. Lazarides, M. P. Sorensen, A. V. Ustinov, N. F. Pedersen, and V. A. Oboznov, J. Appl. Phys. **79**, 7854 (1996).

[12] S. Keil, I. V. Vernik, T. Doderer, A. Laub, H. Prebler, R. P. Huebener, N. Thyssen, A. V. Ustinov, and H. Kohlstedt, Phys. Rev. B **54**, 14 948 (1996).

[13] M. D. Fiske, Rev. Mod. Phys. **36**, 221 (1964).

[14] I. O. Kulik, Sov. Phys. Tech. Phys. **12**, 111 (1967).

[15] N. Grønbech-Jensen, P. S. Lomdahl, and M. R. Samuelsen, Phys. Lett. A **154**, 14 (1991).

[16] B. D. Josephson, Phys. Lett. **1**, 251 (1962).

[17] N. Grønbech-Jensen, P. S. Lomdahl, and M. R. Samuelsen, Phys. Rev. B **43**, 12 799 (1991).

[18] A. Barone and G. Paternò, *Physics and Applications of the Josephson Effect* (Wiley, New York, 1982).

[19] K. Schwidtal and C. F. Smiley, in *Low Temperature Physics–LT13*, edited by K. D. Timmerhaus, W. J. O'Sullivan, and E. F. Hummel (Plenum, New York, 1974), Vol. 4, p. 575.

[20] M. Girillo, G. Costabile, S. Pace, and B. Savo, in *Low Temperature Physics–LT17*, edited by U. Eckern, A. Schmid, W. Weber, and H. Wuhl (Elsevier, New York, 1984), Vol. 4, p. 475.

[21] H. Kroger, L. N. Smith, and D. W. Jillie, Appl. Phys. Lett. **39**, 280 (1981).

[22] J. G. Gijsbertsen, E. P. Houwman, J. Flokstra, H. Rogalla, J. B. le Grand, and P. A. J. de Korte, IEEE Trans. Appl. Supercond. **3**, 2100 (1993).

[23] A. Oliva and R. Monaco, IEEE Trans. Appl. Supercond. **4**, 25 (1993).

[24] G. Costabile, S. Pagano, and R. D. Parmentier, Phys. Rev. B **36**, 5225 (1987).

[25] R. Monaco, G. Costabile, and N. Martucciello, J. Appl. Phys. **77**, 2073 (1995).

[26] G. Paternó and J. Nordman, J. Appl. Phys. **49**, 2456 (1978).